Research Article

Journal of PeptideScience

Received: 2 April 2008 Revised: 5 August 2008 Accepted: 29 August 2008 Published online in Wiley Interscience: 26 November 2008

(www.interscience.com) DOI 10.1002/psc.1078

Improving the interaction of Myc-interfering peptides with Myc using molecular dynamics simulations

Eva M. Jouaux,[a] Barbara B. Timm,[a] Katja M. Arndt,[a,b,c]* and Thomas E. Exner[d]**

Previously, a Myc-interfering peptide (Mip) was identified for the targeted inactivation of the Myc : Max complex by the combination of rational design and an *in vivo* protein-fragment complementation assay. In the subsequent work presented here, molecular dynamics simulations and free energy calculations based on the molecular mechanics GBSA method were performed to define the contribution of the different amino acids in the Myc : Mip coiled coil domain, and compared to wild-type Myc : Max. For further optimization of the Myc interference, point mutations were introduced into Mip and analyzed, from which two showed much higher binding affinities in the computational studies in good agreement with the experiment. These mutants with very high potential for inactivation of Myc can now be used as starting point for further optimizations based on the computational as well as experimental protocols presented here.

Keywords: oncogene; leucine zipper; bHLHZip motif; circular dichroism; free energy calculations

Introduction

Myc belongs to the Myc-Max-Mxd (the last is also known as Mad) transcription network. It is one of the most frequently deregulated oncogenes in human cancers [1–3], and even its brief inactivation is sufficient to induce tumor regression, tumor loss or tumor dormancy in some cancers [4–7]. Hence, the targeted inactivation of Myc provides a novel therapeutic opportunity and challenge. The transcription regulatory functions and oncogenic transformation activities of Myc require its heterodimerization with Max and binding to E-Box DNA sequences (reviewed in [1,8–13]). Myc alone homodimerizes very poorly [8,9]. Beside its cancerous activity Myc has been shown to be involved in normal cell activities, like proliferation, apoptosis, metabolism and differentiation [1,14–17]. Myc belongs to the bHLHzip class of proteins, which consist of two α-helices separated by a loop. The *N*-terminal α-helix is composed of the basic DNA binding region and of helix 1 of the HLH motif; the second α-helix includes helix 2 and the leucine zipper. Helix 1 is not involved in the specificity of dimerization; this is dictated via the helix 2 leucine zipper only [18]. *N*-terminal of the bHLHzip domain of Myc is the transactivation domain (TAD).

Leucine zippers are a subclass of dimeric parallel coiled coils [19–24]. The coiled coil protein motif, first described by Crick in 1953 [25], is widespread in nature; approximately 3–5% of all amino acids encoded in proteins are predicted to form a coiled coil motif [26]. Coiled coils are characterized by a heptad repeat (denoted a–g) (Figure 1). The hydrophobic core at the interhelical interface is formed by residues of positions **a** and **d** [27]. In parallel dimeric leucine zippers, position **a** generally favors β-branched amino acids, whereas position **d** is usually occupied by L [27–30]. Positions **e** and **g** form the edge of the interface and often contain charged or polar residues such as E, Q, K or R, which are generally placed to be complementary to one another, allowing for beneficial interhelical salt bridges in a $\mathbf{g}_i$ and $\mathbf{e}'_{i+1}$ manner (where $\mathbf{g}_i$ denotes the **g** position of one heptad and $\mathbf{e}'_{i+1}$ the **e** position of the following heptad of the other strand) [31–34]. These interactions can add to the stability of the dimer which is mainly brought about by the hydrophobic interactions upon the burial of hydrophobic side chains at positions **a** and **d** of the dimer interface ([35–37] and references therein). Positions **b, c**, and **f** are solvent-exposed and mostly occupied by polar residues that aid in enhancing protein solubility. These three positions have been shown to be variable within the protein sequence. They may also play a further role in stabilizing the coiled coil by, e.g.

* *Correspondence to: Katja M. Arndt, Department of Biology and Center for Biological Signaling Studies (bioss), University of Freiburg, Schaenzlestr. 1, D-79104 Freiburg, Germany. E-mail: katja@biologie.uni-freiburg.de*

** *Thomas E. Exner, Juniorprofessor für Theoretische Chemische Dynamik, Department of Chemistry, University of Konstanz, D-78457 Konstanz, Germany. E-mail: thomas.exner@uni-konstanz.de*

a *Department of Biology, Albert-Ludwigs University Freiburg, D-79104 Freiburg, Germany*

b *Center for Biological Signaling Studies (bioss), Albert-Ludwigs University Freiburg, D-79104 Freiburg, Germany*

c *FRIAS, School of Life Sciences, LIFENET, Albert-Ludwigs University Freiburg, Albertstraße 19, D-79104 Freiburg, Germany*

d *Department of Chemistry and Zukunftskolleg, University of Konstanz, D-78457 Konstanz, Germany*

Abbreviations used: *bHLHZip, basic-helix-loop-helix-zipper motif; CD, circular dichroism; GBSA, generalized Born/surface area; MD, molecular dynamics; Mip, Myc-interfering peptide.*

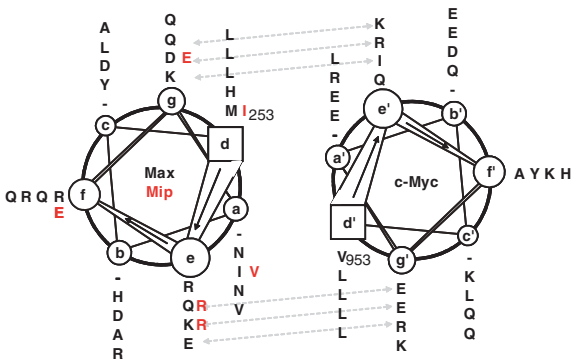

Figure 1. Helical wheel projection of the Myc : Max leucine zipper and the Mip sequence, looking down the helix axis from the *N*-terminus to the *C*-terminus. Wild-type amino acids of the Myc and Max leucine zipper region are given in black, and residues of Mip are red. Peptides start with position ***d***, hence there are no ***a, b***, and ***c*** positions in the first heptad (marked with −). Position ***f1*** of Mip was changed to E for additional N-cap stability, and position ***c2*** of Max and Mip, as well as position ***f2*** of Myc, were changed to Y to assist with concentration determination. Numbers at positions ***d1*** and ***d'1*** refer to the numbers in 1NKP entry from PDB.

intrachain electrostatic interactions or interactions with the helix macrodipole [38].

We reported previously [39] the targeted inactivation of the Myc : Max complex with the interfering peptide Mip identified by a combination of rational design and an *in vivo* protein-fragment complementation assay [37,40]. The selected Mip differs in only 5 out of 29 amino acids from the Max leucine zipper sequence. As the leucine zipper alone only showed poor stability, and since we were interested in inhibiting the human wild-type interaction, we added the native basic DNA binding region and the HLH motif, abbreviated with bMyc and bMax. In the case of Mip, the basic region was replaced by an acidic extension (resulting in aMip) that interacts with the basic region of human Myc in order to further abolish DNA binding. This acidic extension has been reported to interact with the basic domain of Myc [41,42]. The bMyc : aMip complex outcompetes the wild-type bMyc : bMax interaction and interferes with DNA binding. The T_m of bMyc : aMip interaction is 13 °C higher compared to the wild-type bMyc : bMax complex [39].

In this paper, we performed MD simulations and free energy calculations based on the molecular mechanics (MM)-GBSA method, in order to define the contribution of the different amino acids in the Myc : Mip coiled-coil complex and compare it to the wild-type Myc : Max. From these results, we created and analyzed Mip mutants with even better Myc interaction characteristics. Studies describing similar simulations of coiled coils have already been published [43–50]. The earliest simulations were performed by Offer and Sessions [43] analyzing the lowest-energy conformations of leucine in the inner core of the interface of a two-stranded coiled coil. Another early paper [44] describes the folding thermodynamics of the GCN4 leucine zipper. Charest and Lavigne suggest a simple but versatile set of restraints to generate structures of coiled coils with different strandedness starting from separated α-helices [45]. In addition, a number of stability studies on specific systems were carried out, e.g. on specially designed, synthetic coiled coils [46,47], the GCN4 leucine zipper [47], or wild-type and mutated α-Keratin [48]. In the last investigation, changes in free energy were calculated by the thermodynamic integration approach. Analysis on the configurational entropy of a trimeric coiled coil were conducted in [49] demonstrating the importance of salt bridge networks for thermostability. In a very recent publication [50], a potential switching mechanism in an α-helical coiled coil was proposed and verified with MD simulations. The goal of the work presented here was to improve the interactions of Myc with Mip by introducing additional point mutations. The differences between the Myc : Max and Myc : Mip complexes were characterized, and three point mutations were suggested and analyzed for increased binding affinities.

Materials and Methods

Molecular Dynamics Simulations

For further optimization of the interactions between the best experimentally determined polypeptides Mip and Myc, theoretical investigations were performed on the basis of molecular dynamics simulations. In these simulations, interface point mutations of Mip were generated and the binding energies of the complexes with Myc, calculated with the MM-GBSA method, were compared to the Myc-Mip as well as to the Myc-Max complex. For these calculations, the protocol proposed by Gohlke *et al*. [51–53] was applied.

Molecular mechanics – generalized born/surface area (MM-GBSA)

Following the MM-GBSA approach [54,55], binding free energies were calculated according to

$$\Delta G_{\text{binding}} = \langle G^{\text{complex}}(i) - G^{\text{protein1}}(i) - G^{\text{protein2}}(i) \rangle_i \qquad (1)$$

where $\langle\ \rangle_i$ denotes an average over snapshots i taken from MD simulations. Free energies of the complex $G^{\text{complex}}(i)$ as well as the unbound molecules $G^{\text{protein1}}(i)$ and $G^{\text{protein2}}(i)$ were estimated from contributions of gas-phase energies and solvation free energies:

$$G^x(i) = H^x_{\text{gas}}(i) + H^x_{\text{trans/rot}}(i) + G^x_{\text{solvation}}(i) - TS^x(i) \qquad (2)$$

In Eqn (2), gas-phase energies $H^x_{\text{gas}}(i)$ were calculated using the Cornell *et al*. force field [56] summing up contributions from internal (bond, angle, torsion angle energies), electrostatic, and van-der-Waals energies. In the classical limit, the energy $H^x_{\text{trans/rot}}$ (i) is a constant of 3RT due to six translational and rotational degrees of freedom and could thus be omitted for the calculation of relative binding free energies, but was included due to its simplicity. Solvation free energies $G^x_{\text{solvation}}(i)$ were calculated as a sum of polar and nonpolar contributions.

$$G^x_{\text{solvation}}(i) = G^x_{\text{polar}}(i) + G^x_{\text{nonpolar}}(i) \qquad (3)$$

The modified generalized Born (MGB) model [57] as implemented in AMBER 8.0 was used for the polar part. The parameters were set according to the description of Gohlke *et al*. [51]. The nonpolar part due to cavity formation and van-der-Waals interactions between the solute and the solvent was approximated by a solvent accessible surface area (SA) term also following the description of Gohlke *et al*. [51]:

$$G^x_{\text{nonpolar}}(i) = \gamma \cdot SA^x(i) \qquad (4)$$

Snapshots were extracted every 20 ps from the last 3 ns of the production runs (see below). All water molecules and counterions were stripped. Note that the estimates for the unbound proteins were also based on the MD simulations of the complex. Due to the flexibility of the molecules and the instability of the single

α-helices in solution, this is only a very rough approximation. A large amount of the reachable configuration space of the unbound molecules is not sampled resulting in too high free energies for the components and, therefore, too favorable binding free energies. However, we think that these errors canceled out when two different mutations are compared, so that the qualitative trend can be reproduced by the calculations. This is sufficient for the purpose of this study, which is to guide experimental investigations and not to quantitatively reproduce binding free energies. In this sense, we also did not consider the contribution of entropic parts $TS^x(i)$ to the binding free energies, because these will also be very error prone. Even if Missimer *et al*. [49] pointed out the importance of salt bridge networks on configurational entropy, we anticipate that the changes introduced by the mutations on these networks are minor and that their entropic contributions almost cancel out in relative binding free energies.

Free energy decomposition

One advantage of the MM-GBSA method is that not only total binding free energies can be calculated but these binding free energies can also be decomposed into the components resulting from individual residues [51], providing insight into the origin of binding on an atomic level. The parts of the free energy $G^x(i,j)$ associated with a specific residue j contain contributions from internal gas-phase energies, solvation free energies, and entropies [51]:

$$G^x(i,j) = H^x_{\text{gas}}(i,j) + G^x_{\text{solvation}}(i,j) - TS^x(i,j) \quad (5)$$

As previously, we neglected the entropic parts for our qualitative investigations. Gas-phase energies were either added fully to $G^x(i,j)$, if all atoms contributing to the specific bond, angle, or torsional angle were part of residue j, or they were split among multiple residues according to the number of atoms that belong to each residue. Similarly, one half of the energy for van-der-Waals interactions and gas-phase electrostatic interactions were added to the free energy of those residues to which the interacting atoms belonged. The electrostatic fraction of the solvation free energy for each amino acid was calculated according to

$$G^x_{\text{polar}}(i,j) = -\tfrac{1}{2}\sum_{u\in j}\sum_{v}\left(1 - \frac{\exp(-\kappa f^{\text{GB}}_{\text{uv}}(r_{\text{uv}}))}{\varepsilon_w}\right)\cdot\frac{q_u q_v}{f^{\text{GB}}_{\text{uv}}(r_{\text{uv}})} \quad (6)$$

where κ is the Debye-Hückel screening parameter, ε_w is the dielectric constant of water, and f^{GB} is a function that depends on the atomic radii and the distance between the atoms. The ionic strength was set to 0 mM for simplicity. The solvent accessible surface area per atom and, in this way, the nonpolar part of the solvation free energy were estimated with the LCPO algorithm [58].

Simulation details

The simulations were performed following the protocol of Gohlke *et al*. [51–53]. The AMBER 8 suite of programs [59] with the modified version of the Cornell *et al*. force field [56] (parm99) was used. The structure of the Myc : Max complex was taken from the Protein Data Bank [60] (PDB entry 1NKP), and amino acids 947–980 of Myc (chain A), and 247–280 of Max (chain B) were extracted. This corresponds to the leucine zipper region of the complex, which was also investigated by the experimental rational design/*in vivo* selection study [39]. The fragments were then capped by acetyl starting groups at the *N*-Termini and *N*-methylamine ending groups at the *C*-termini. The mutations were done by removing the side chain of the residue and renaming the residue entry of the backbone atoms in the PDB file. During the preparation of the input files for the molecular dynamics simulations (program leap [59]), the missing atoms were added in standard position. These starting structures were placed in a periodic truncated octahedron of TIP3P water molecules [61] and counterions were added to provide a physiological ionic strength (150 mM) and maintain electroneutrality of the system. The borders of the truncated octahedron were chosen to be at least 12 Å from every solute atom.

The system was minimized for 8000 steps to relax unfavorable conformations generated by the standard placement of the missing atoms. The particle mesh Ewald (PME) method [62] was used to treat long-range electrostatic interactions, and the SHAKE method [63] to constrain bond lengths of bonds involving hydrogen atoms. The time step for all MD simulations was set to 2 fs with a nonbonded cutoff of 12 Å. For equilibration, the system was first heated from 100 K to 300 K for 40 ps and then relaxed to the density corresponding to 1 bar for 300 ps in a sequence of MD simulations using the canonical (NVT) and the isothermal isobaric (NPT) ensemble, respectively. In these simulations, harmonic restraints with force constants of 5 kcal mol^{-1} Å^{-2} were applied to all C_α atoms. These restraints were then gradually reduced to zero during 700 ps of NVT-MD. The following production simulation (NVT) of 7 ns was divided into one part for further equilibration of the system (4 ns), and the remaining part for extracting the snapshots for binding free energy calculations and free energy decomposition (3 ns).

Experimental Work

Protein sequence, cloning, and expression

Human bHLHZip Myc and Max sequences consist of the basic DNA binding region (underlined), the helix-loop-helix (HLH) region, and the leucine zipper (Zip) domain (bold) followed by a hexa-histidine tag (bMyc: NVKRRTHNVLERQRRNELKRSFFALRDQLPELENNEKAPKV VILKKATAYILS**VQAEEQKLISEEDLLRKRREQLKHKLEQL**GAPHHH HHH; bMax: ADKRAHHNALERKR RDHIKDSFHSLRDSVPSLQGEKA SRAQILDKATEYIQY**MRRKNHTHQQDIDDLKRQNALLEQQVRAL** GAPHHHHHH). In aMip, the basic region of bMax (underlined) is replaced with an acidic extension (PDEEEDDEEELEELED) designed by Krylov *et al*. [41,42]. The leucine zipper regions of bMax and aMip differ only in the amino acids indicated in Figure 1. The respective sequences were encoded in pQE-16 (Qiagen) vector derivatives [39]: pAR200d-bHLHMyc, pAR200d-bHLHMax, pAR200d-aHLHMip.

Mip mutants were created by site-directed mutagenesis and cloned using *Nhe*I and *Hin*dIII restriction enzymes (NEB) into the expression vector pAR200d-aHLHMip (described in our previous publication [39]) to yield the plasmids pAR200d-aHLHMipH260L, pAR200d-aHLHMipV264I and pAR200d-aHLHMipR279Q. The following primers were used: prMipI/Q-fwd: AGGCAGGAAATTGAT GACCT, prMipI-rev: AGGTCATCAATTTCCTGCCT, prMipQ-rev: TGAA GGCGCGCCTAACGCTTGAACTTGCTGTTCCAGCAG, prMipL-fwd: ATCATTATCTCCGGCAGGA, prMipL-rev: TCCTGCCGGAGATAAT-GATT. For the PCR reactions, the reaction mixtures (50 µl) contained 50–100 ng template, 2.5 U *Taq* polymerase (Genaxxon), 1.5 mM $MgSO_4$, 1× polymerase buffer, primers (each 25 pmol), and dNTPs (0.4 mM per dNTP), and the two following programs were used: Program 1) 3 min 94 °C followed by 28 cycles of 1 min 94 °C, 1 min

44 °C, 1 min 72 °C, and 1 cycle of 7 min 72 °C. Program 2) 3 min 94 °C followed by 28 cycles of 30 s 94 °C, 20 sec 44 °C, 40 s 72 °C, and 1 cycle of 4 min 72 °C. Cloned sequences were verified by sequencing.

Protein expression was performed in *E. coli* BL21 with pRep4 (Qiagen) at 30 °C in 2YT medium (10 g/l yeast extract, 16 g/l bacto tryptone, 5 g/l NaCl). Induction with 1 mM IPTG was performed after 1.5 h of incubation, and proteins were expressed for 7–9 h.

Protein Purification

Protein purification by affinity chromatography

His_6-tagged proteins were purified with a self-packed column containing 1 ml of Ni-NTA superflow (Qiagen). The expression culture pellet of bMax, aMip, and aMip variants was resuspended in 20 ml binding buffer (50 mM Na-phosphate, 150 mM NaCl, pH 7.2), sonified and centrifuged. The filtered (0.45 µm) supernatant was loaded manually on the column equilibrated with 3 column volumes (CV) of binding buffer. The column was washed with 5 CV binding buffer and 5 CV wash buffer (50 mM Na-phosphate, 300 mM NaCl, 20 mM imidazol, pH 7.2). Elution of proteins was performed with elution buffer (50 mM Na-phosphate, 300 mM NaCl, 250 mM imidazol, pH 7.2). For the purification of bMyc denaturating conditions were chosen due to low yields with the upper procedure. The pellet was resuspended in denaturing binding buffer (100 mM NaH_2PO_4, 10 mM Tris base, 8 M urea, pH 8.0). For the purification, the same column was used but equilibrated with denaturing binding buffer. The protein was refolded on the column using 4 CV denaturing binding buffer, 4 CV denaturing wash buffer (100 mM NaH_2PO_4, 10 mM Tris base, 8 M urea, pH 6.3), 4 CV 1 : 1 mixture of denaturing wash buffer and binding buffer (see above), 4 CV binding buffer. Elution of the protein was performed with elution buffer mentioned above.

Protein purification by reversed-phase chromatography

Proteins obtained from Ni-NTA affinity purification were further purified by reversed-phase high-performance liquid chromatography (RP-HPLC) using a Jupiter Proteo column (4 µm particle size, 90 Å pore size, 250 × 10 mm; Phenomenex). The column was equilibrated at 20% acetonitrile (ACN), 0.1% TFA. A linear gradient of ACN in water, both containing 0.1% TFA, was used from 20 to 50% in 60 min with a flow rate of 1 ml/min (0.5%/min). Obtained proteins were lyophilized with a speed-vac and dissolved in water. Correct masses were verified by electrospray mass spectrometry. Peptide concentrations were measured in water using absorbance at 280 nm and peptide-specific extinction coefficients.

Circular dichroism spectroscopy

Circular dichroism measurements were carried out with a temperature-controlled Jasco J-810 circular dichroism spectrapolarimeter. A quartz cuvette with 0.5 mm path length was used. Spectra were obtained from samples containing 4.8 µM of each protein in CD buffer (10 mM K-phosphate, 100 mM KF, pH 7), and three scans were averaged. Temperature denaturation profiles were recorded at a constant wavelength of 222 nm from −8 to 85 °C, respectively, with a ramp at a rate of 0.6 °C/min. All profiles were found to be >90% reversible. Temperature denaturation measurements were highly reproducible, and resulting T_m values usually varied by not more than ±0.5 °C (data not shown). Apparent T_m values were determined by least-squares curve fitting of equilibrium denaturation curves [35–37,64] assuming a two-state model of a folded peptide dimer unfolding to a monomer, a model which is well established and valid for most coiled coils [38,65–67].

Results and Discussion

Structural and Energetical Comparison of the Myc : Max and Myc : Mip Complexes

MD simulations of the Myc : Max and the Myc : Mip complexes were performed as described in the Materials and Methods section with a production run of 7 ns, from which the last 3 ns were used for analysis. First, the simulations were studied by the generation of average structures (Figure 2) and by the time series of the root mean square deviations (rmsd) of the backbone atoms from this average structure (Figure 3(a)). For the visualization, the average structure was minimized to get reasonable atomic distances and angles. In this way, prominent intermolecular interactions and the flexibility of the system can be inspected. It is obvious from Figure 3(a) that the Myc : Max as well as the Myc : Mip complex are very flexible making further investigations on the basis of these simulations impossible (see below) due to the problem of incomplete sampling. This large flexibility can be mainly attributed to the termini, especially the *N*-termini, of the two complex partners. To show this, we calculated the rmsd of the *N*-terminal, the *C*-terminal and the central amino acids separately as shown in Figure 3(b) and (c). Small rmsd values below 2 Å are computed for the central part, whereas the *C*- and *N*-termini show deviations of up to 5 Å and 11 Å, respectively.

The large flexibility of the termini can be explained by the many polar and charged side chains in these regions. These can build strong valuable interactions with other polar or charged side

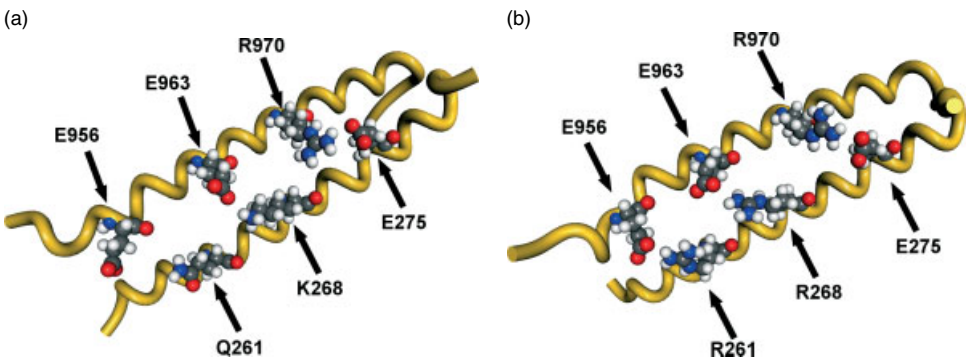

Figure 2. Average structure of (a) the Myc : Max, and (b) the Myc : Mip complex taken from the last 3 ns of a 7-ns-long production run. Three important interactions stabilizing the complexes are shown in spacefill (CPK) representation.

Journal of PeptideScience

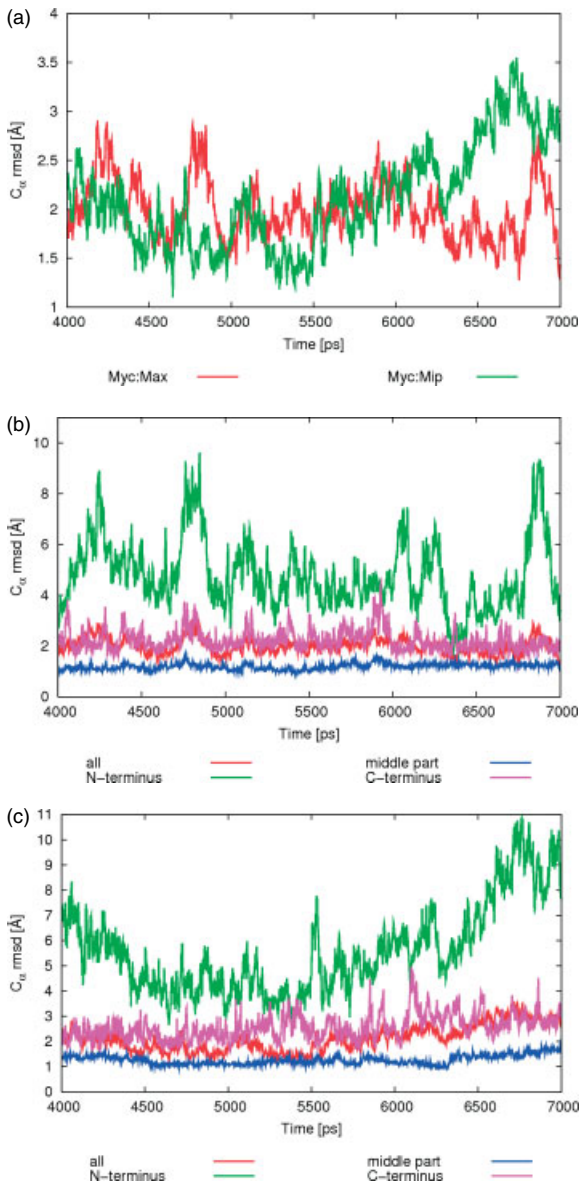

Figure 3. Time series of the root mean square deviation of the C_α-atoms in the Myc : Max and Myc : Mip complexes (a) and for different parts of the Myc : Max (b) and Myc : Mip complexes (c).

chains but also with the very polar solvent water. Additionally, there is almost no hydrophobic core stabilizing these parts of the complex. In this way, there are many, energetically very similar but structurally diverse, conformations leading to partial unfolding of the α-helices and to a partial destruction of the complexes. This instability of the simulation is not an artifact of the force field. In the biological complex, the leucine zipper region is extended at the *N*-termini by the helix-loop-helix and basic DNA binding regions. The Myc : Max leucine zipper domains alone are very unstable also in the experiment (experimental data not shown). The additional domains (basic region and HLH motif), especially when bound to the DNA, strongly stabilize the complex and make it more rigid. The acidic extension to Max and Mip is fulfilling the same purpose in the CD measurements.

We then used the MM-GBSA method as described above to also compare the energetical differences between the Myc : Max and Myc : Mip complex. We will only discuss the results qualitatively, because of the limitations of the simulations described in the Materials and Methods section (energies of unbound partner taken from the complex simulations, generalized Born solvent model, neglect of entropic contributions). Especially because of the first reason, the calculated absolute binding free energies are expected to be highly overestimated. The binding free energy was calculated and averaged over 1500 snapshots of the last 3 ns using the MM-GBSA approach. This resulted in values of 64.48 ($\pm$8.34) and 64.82 ($\pm$8.14) kcal/mol for the Myc : Max and the Myc : Mip complex, respectively. The standard deviations are given in parentheses. Due to the large error bars resulting from the flexibility of the molecules, these two energies must be considered as equal. A second simulation of the Myc : Mip complex from a different starting conformation produced a much more favorable binding free energy of $-$76.89 ($\pm$6.32) kcal/mol. However, it is still not clear if the more favorable binding free energy is a result of the differences in Max and Mip or if it just appears by chance due to better interactions in the terminal regions during the sampling period. Nevertheless, some prominent differences between the Myc : Max and the Myc : Mip complexes can be seen in the averaged structure even in the first simulation (Figure 2). One new salt bridge is built between E956 of Myc and R261 of Mip. Additionally, the salt bridge between E963 of Myc with K268 in Max is substituted by a stronger one with R268 in Mip. The free energy decomposition into the components of individual residues confirms the importance of the Q261R and K268R mutations (data not shown). In both cases, the R shows a much larger contribution to the binding affinity than the corresponding residues in the original complex. The fact that this does not lead to a more favorable total binding free energy in the first simulation can, as already mentioned, be attributed to parts, in which Max and Mip have the same amino acid sequence, i.e. in which no mutations were experimentally introduced. Even if these parts should behave very similar in the two structures, this is not the case because of the flexibility and resulting sampling problems. For example, K256 has a much larger contribution to the binding affinity in the Myc : Max than in the Myc : Mip complex, which can be explained by a salt bridge between E957 and K256 formed 84% of the time in the Myc : Max complex, but less than 20% of the time in the Myc : Mip complex.

The large energy differences between the two simulations of Myc : Mip demonstrate that the results obtained by the unconstraint simulations are very unreliable. Due to the fact that the structural diversity of the termini and the resulting uncertainty in the energetics of these parts can easily hide the influence of the mutations on the binding free energy, additional simulation of the mutations on this basis are almost certain to fail (simulation of point mutations of Mip showed totally uncorrelated binding free energies, data not shown). Extending the leucine zipper as done in the experiment is not an option because of the increasing demand on computer time. To circumvent these problems and to keep the simulations as good as possible, we tried to enforce the coiled coil structure on the simulation by distance and position restraints. In the first approach, we followed the ideas of Charest and Lavigne [45], who were able to generate coiled coil structures from separated α-helices by interhelical distance restraints between C_α at the interface positions **a** and **d**. For each corresponding **a**–**a**′ and **d**–**d**′ pair, no penalty is applied up to a C_α–C_α distance of 8 Å. If the distance increases further, a parabolic potential with a force constant of 20.0 kcal mol^{-1} Å^{-2} is used up to a distance of 8.5 Å. After that, a linear potential is applied

with the slope of the parabola at 8.5 Å. In a second approach, we tried to simulate the fact that the *N*-termini are more constraint in the experiment due to the interaction of the basic and acidic extensions. As already mentioned, these long extensions cannot be modeled in a reasonable amount of computer time. Therefore, we modeled the effect by position restraints on the C_α of the first and last four amino acids of each chain. A harmonic potential was used forcing the atoms back to their original position with a force

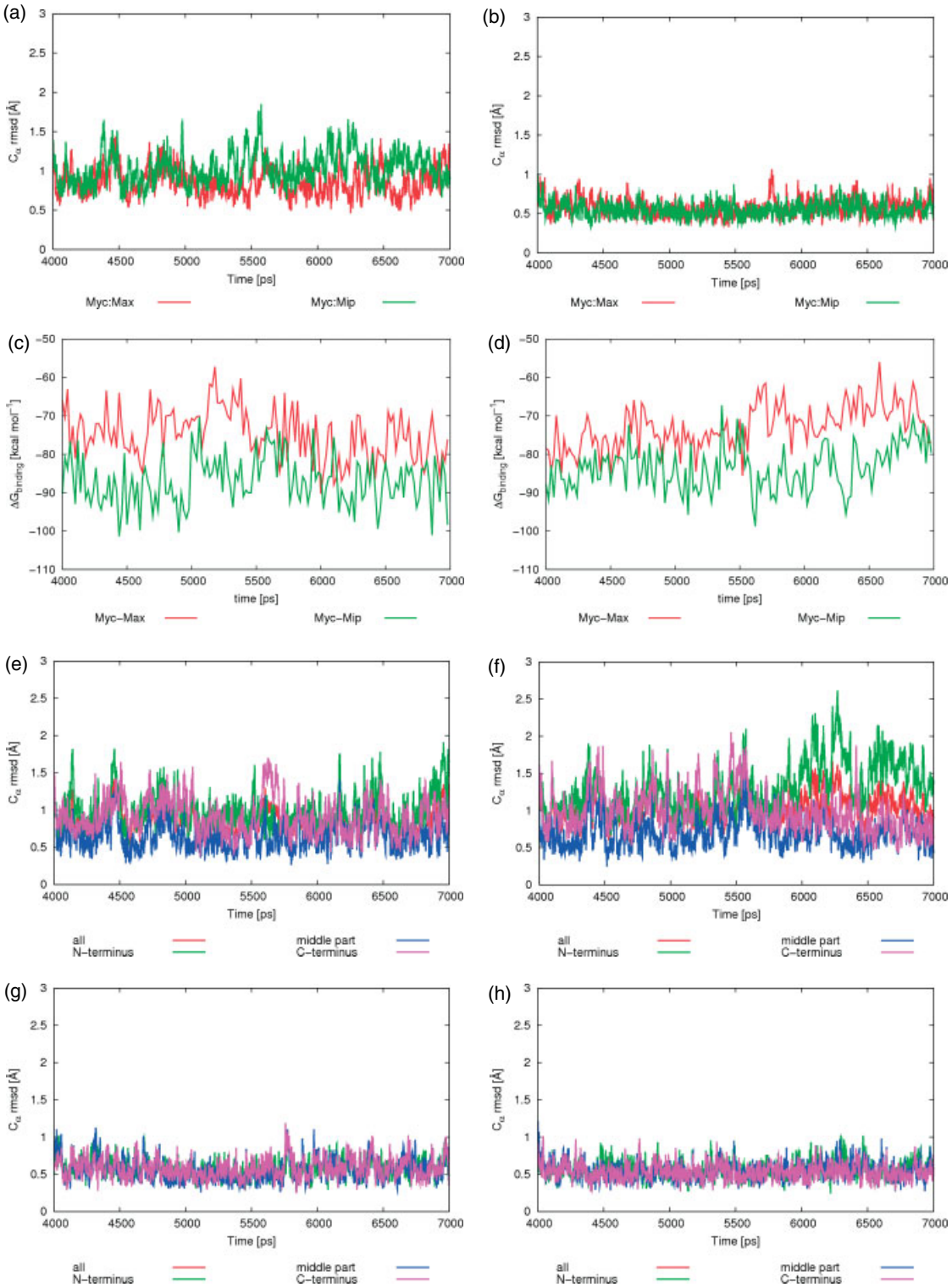

Figure 4. Time series of the root mean square deviation of the C_α-atoms (a, b) and the binding free energy (c, d) in the Myc : Max and Myc : Mip complexes taken from the simulations using (a, c) distance restraints and (b, d) position restraints. Time series for different parts of the (e, g) Myc : Max and (f, h) Myc : Mip complexes from the simulation using distance restraints (e and f) or position restraints (g and h).

constant of 1.0 kcal mol^{-1} Å^{-2}. This small force constant was used to minimize the artificial influence on the central parts of the chains, in which the structure should have the freedom to adapt under the influence of the mutations. As can be seen in Figure 4, both sets of restraints fulfill their purpose to remove the large flexibility of the termini. In the case of the **a**–**a**′ and **d**–**d**′ distance restraints, the rmsd of all C_α positions is in almost all time steps below 2 Å, and the ones of the *N*- and *C*-terminal parts do not exceed 2.5–3 Å, an extreme decrease from up to 11 Å in respect to the unconstraint simulations. For the position restraints, the rmsd values are even smaller. This is not only the case for the termini, where the rigidity is enforced by the restraints, but also in the middle parts of the molecules. Overall, both sets of restraints produced a stable simulation well representable with one average structure and much increased probability to obtain reproducible binding free energies with relatively short, practicable simulation times.

MM-GBSA calculations using the new simulations resulted in binding free energies of −74.81 (±6.51) and −72.87 (±5.67) kcal/mol for the Myc : Max complex, and −86.99 (±6.35) and −83.68 (±5.81) kcal/mol for the Myc : Mip complex using the distance and positions restraints, respectively (the binding free energies for each snapshot can be seen in Figure 4 as time series). Thus, for both restraints sets, an increase in the binding affinity of over 10 kcal/mol when going from Max to Mip is obtained. For an indepth investigation of the increased binding affinity, we calculated the per-residue contribution. For space saving reasons, we only discuss the results of the position-restraint simulations in detail here. The distance constraints results draw a very similar picture. The contributions are shown color-coded on the molecular surface of Max and Mip in Figure 5(a) and (b), respectively.

As already discussed, the main increase in binding affinity can be attributed to the two new R residues at positions 261 and 268 (dark blue regions in Figure 5). From the other three point mutations (M253I, D263E, and I264V), only the M253I shows a very minor positive influence on the binding affinity. It is a little surprising that residue 263 has almost no contribution to the binding energy. D in Max as well as E in Mip are able to form a salt bridge with MycR968. But, it seems that this bridge is not very stable. It is therefore not formed and the residues interact more favorably with the surrounding water most of the time. All other amino acids give almost the same contributions in both complexes, which give us the confidence that the sampling time is long enough for the constraint systems to sample the important conformational space. Consequently, it should be possible to see the influences of additional point mutations for the further improvement of the interfering peptide.

Further Improvement of the Myc : Mip Complex by Point Mutations

As described in detail in the Materials and Methods section, the calculated absolute binding free energies are not expected to be very accurate, due to the limitations of the simulation caused by the large flexibility of the molecules, especially the monomers, not accounted for in the simulations. Nevertheless, these errors should be similar for highly related systems and cancel out when calculating energy differences. If this is the case, simulations can be used to further improve the interfering peptide by repeating the calculations with point mutants of Mip and identifying those with improved binding. Three point mutations were chosen for the simulations and subsequent experimental validation. The main reason for the instability of the Myc : Max complex is the limited interaction area of the hydrophobic core. Therefore, two mutations (MipV264I and MipH260L) were introduced to increase the hydrophobic contacts. The aim of the third mutation MipR279Q was to increase the electrostatic interaction between the two partners of the complex. A salt bridge is formed between MycR970

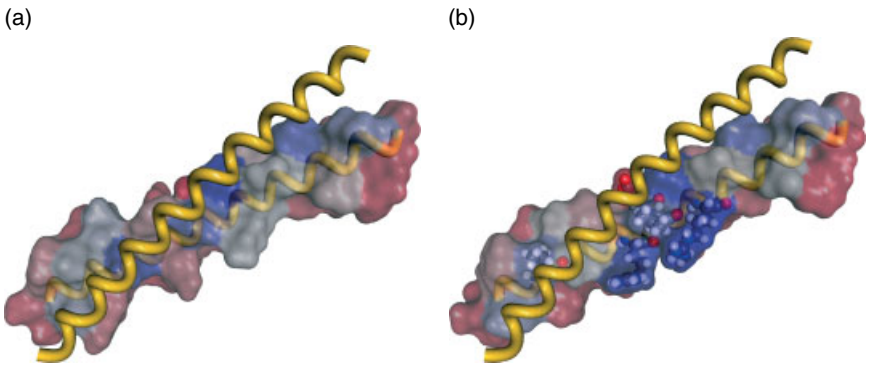

Figure 5. Decomposition of the binding free energy taken from the position-restraint simulations into the components of individual residues of the Myc : Max (a) and Myc : Mip (b) complexes mapped onto the molecular surface of Max and Mip, respectively. Blue corresponds to large attractive interactions, and red is for zero contributions. The importance of MipR261 and MipR268 for the increased binding affinity of Myc : Mip can be seen by the darker blue color around these residues.

Table 1. Calculated binding free energy (kcal mol^{-1}) of several point mutations of the Myc : Mip complex for the last 3 ns of a 7-ns-long production run. In addition, the experimentally determined Tm and the ratio of the ellipticity at 222 : 208 nm measured by CD spectroscopy are given

Complex	Myc : Mip	Myc : MipH260L	Myc : MipV264I	Myc : MipR279Q
$\Delta G_{binding}$ (Distance Restr.)	−86.99 (±6.35)	−97.42 (±5.52)	−84.05 (±7.09)	−83.58 (±7.06)
$\Delta G_{binding}$ (Position Restr.)	−83.68 (±5.81)	−90.01 (±4.61)	−93.38 (±5.73)	−84.27 (±6.84)
T_m	46 °C	64 °C	50 °C	42 °C
$\theta_{222\ nm}/\theta_{208\ nm}$	1.1	1.7	1.2	1.5

and MipE275 in the Myc : Mip complex (as well as in the Myc : Max complex). However, because of the closeness of MipR279, MipE275 can also build an intramolecular salt bridge, which probably reduces the strength of the intermolecular one. Therefore, we decided to virtually mutate MipR279 to the noncharged residue, Q, not interacting with MipE275.

The simulations of the mutants were performed in analogy to the Myc : Max and Myc : Mip calculations. Here, distance as well as position restraining resulted in stable simulations with comparable rmsd fluctuations as given above (data not shown) The binding free energies of the point mutations are given in Table 1 for both sets of constraints, including Myc : Mip for comparison. Using distance restraints, only MipH260L leads to an increase of the complex stability in the simulations. When position restraints are used, much more favorable binding energies are obtained for the two mutations enlarging the hydrophobic core. For the MipR279Q mutation the same binding energy (bearing in mind the error bars) was calculated as for the Myc : Mip complex with this second restraint set.

In order to validate which set of restraints gives correct predictions, the three mutations were experimentally tested. Secondary structure and thermal unfolding of the Mip mutants in complexes with Myc and as homodimers were measured by CD spectroscopy. Consistent with published data, the Myc and Max leucine zipper domains alone were very unstable (data not shown). Consequently, as reported [39], we extended the leucine zippers with the human HLH motif and the basic DNA binding region or acidic extension, respectively. The CD spectra of the peptides alone or in various combinations were recorded. All peptides except the homodimers of bMyc and aMipH260L were found to be α-helical (data not shown). Further, the ratio of the ellipticity at 222 nm ($\theta_{222\ nm}$) to the ellipticity at 208 nm ($\theta_{208\ nm}$) was found to be greater than 1.0 (Table 1), indicative of coiled coil formation [68]. Thermal denaturation curves were obtained over a temperature range from $-8\,^{\circ}C$ to $85\,^{\circ}C$ (Figure 6(a)), and T_m values were calculated assuming a two-state transition of the folded dimer to unfolded monomers (Table 1). Compared to the original Myc : Mip interaction ($T_m = 46\,^{\circ}C$), Myc : MipH260L and Myc : MipV264I complexes had higher melting temperatures ($T_m = 64\,^{\circ}C$ and $50\,^{\circ}C$, respectively) indicating higher complex stabilities, whereas Myc : MipR279Q showed a slightly lower stability ($T_m = 42\,^{\circ}C$). Hence, based on the selected Mip, we created two even better interaction partners for human Myc. The increase in the T_m values was $18\,^{\circ}C$ and $4\,^{\circ}C$, respectively, obtained through the change of only one single residue.

Comparing the experimental and theoretical results, it is clear that both constraint sets can predict the experimental trend but give no perfect correlation (Figure 6(b)). However, this is not totally unexpected because of the unphysical constraints needed to confine the available conformational space. One problem is that the flexibility of the system especially when using distance constraints is still large. A possible solution could be decreasing the not-penalized distance of the constraints, which is set to 8 Å at the moment. In contrast, the position constraints are probably too restricting so that not all important conformations are reachable. The largest uncertainty is in the Myc : MipV264I case, in which the position constraints largely overestimate, and the distance constraints underestimate the binding affinity. As shown in Figure 7, this is not a result of different orientations of the mutated

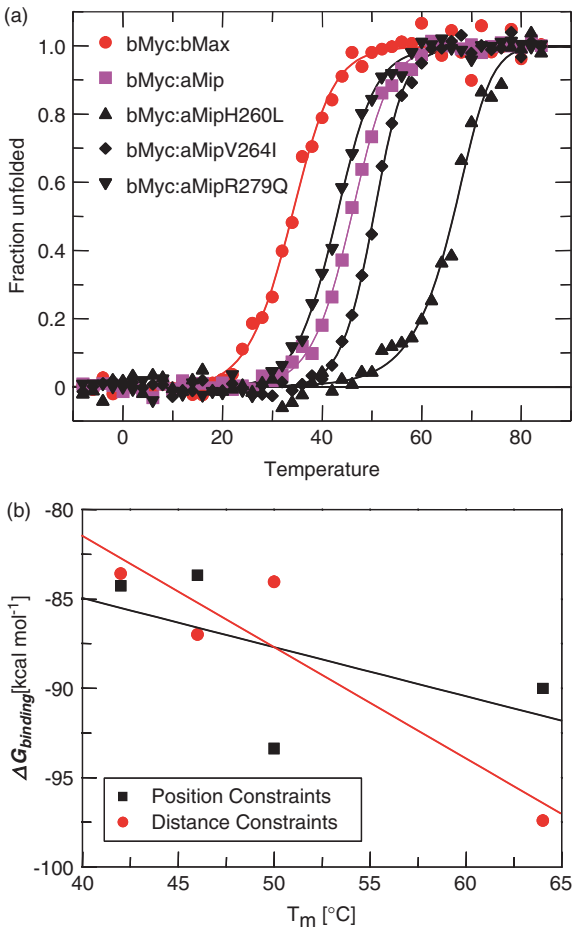

Figure 6. Correlation between measured and calculated binding free energies. (a) Thermal denaturation curves, presented as fraction unfolded, of heterodimers formed by bMyc with bMax (red circles), aMip (pink squares), and aMip-mutants H260L (black triangles), V264L (black diamonds) and R279Q (black inverted triangles). (b) Correlation between the calculated binding free energies and the experimental melting points of several point mutations of the Myc : Mip complex taken from the simulation using position constraints (black squares) and distance restraints (red circles).

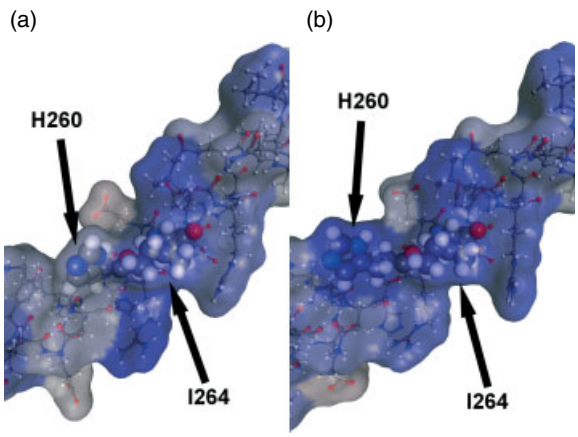

Figure 7. Decomposition of the binding free energy taken from the (a) distance-restraint and (b) position-restraint simulations into the components of individual residues of the Myc : MipV264I, complex, mapped onto the molecular surface of MipV264I. Only the part near the mutation is shown. Blue corresponds to large attractive interactions and red is for zero contributions. The mutated residues as well as the Mip H260, which is most important for the differences in the calculated results, are shown as spacefill (CPK) model.

Journal of PeptideScience

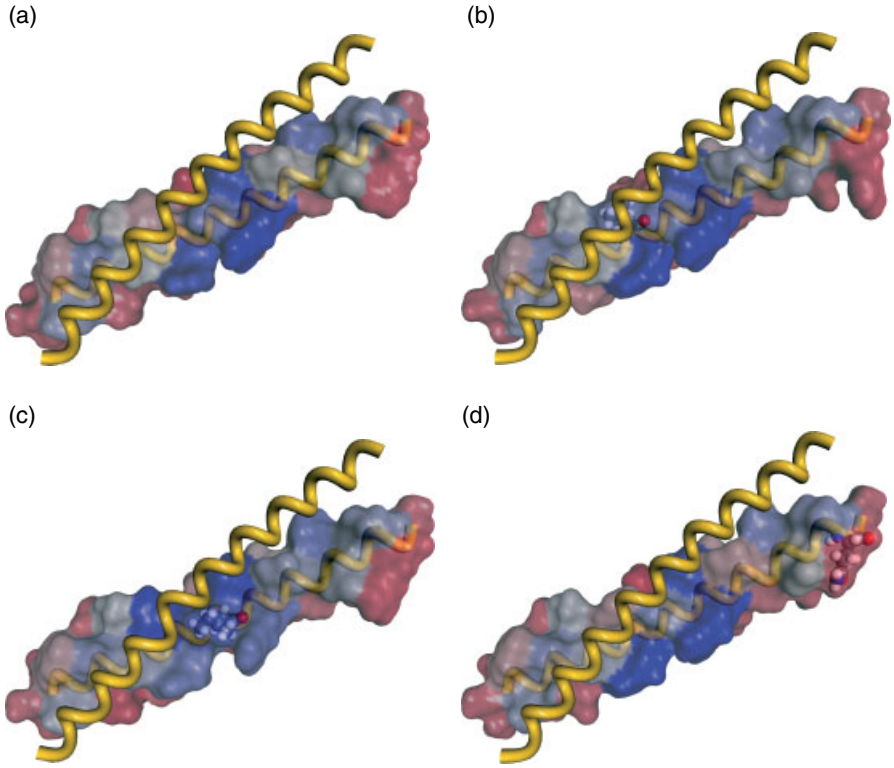

Figure 8. Decomposition of the binding free energy taken from the position-restraint simulations into the components of individual residues of the Myc : Mip (a), Myc : MipH260L (b), Myc : MipV264I (c), and Myc : MipR279Q (d) complexes mapped onto the molecular surface of Mip and its mutations, respectively. Blue corresponds to large attractive interactions and red is for zero contributions. The mutated residues are shown as spacefill (CPK) model.

residue but because of different conformations of the neighboring residue MipH260. The experimental results suggest that the reality lies somewhere in between. Another difficulty with this last mutation is that it was shown in other studies that H260 plays an important role in the heterodimerization of Max with Myc as well as with Mxd [69–73]. It interacts with conserved acidic side chains in all complex partners. Additionally, it is believed that this residue is needed for weakening the interface of the Max homodimer [70,73]. Therefore, this mutation could, on the one hand, limit the heterodimerization with Myc due to the increased stability of the homodimer and, on the other hand, prevent the recognition of Mad. The latter is not problematic for our investigation because we only want to target the Myc : Max interface. Concerning the first objection, the influence of the mutations on the homodimerization will be subject of future investigations.

Nevertheless, the results are well suited to guide the experiment. The mutant with the highest increase in binding affinity was correctly predicted with both simulation protocols. Additionally, the simulations correctly showed that a strengthening of the salt bridge between MycR970 and MipE275 is not possible by removing the positive charge of residue 279 in Mip. That the calculations are reliable can also be seen by mapping the per-residue contributions onto the molecular surfaces (Figure 8). Here also, we show only the results for the position constraints. The distribution looks almost exactly the same, apart from the local regions around the mutations. Thus, the trends in the binding free energies can be assigned to the mutations and are not generated by differences in the interactions over the whole interface caused by the large fluctuations as is the case in the unconstraint as well as distance-constraint simulations. Additional calculations are on their way testing the combination of the two mutations as well as additional mutants following the proposed simulation protocols. These will hopefully lead to even better interactions of the interfering peptide with Myc and, in this way, to the transient inactivation of overexpressed Myc.

Conclusion

In an earlier publication [39], the targeted inactivation of the Myc : Max complex with Mip was reported, identified by the combination of rational design and an *in vivo* protein-fragment complementation assay. In the subsequent work presented here, we performed MD simulations and free energy calculations based on the MM-GBSA method, in order to define the contribution of the different amino acids in the Myc : Mip complex and to compare it to the wild-type Myc : Max interaction. It was clearly shown that the main increase in binding affinity can be attributed to the Q261R and K268R mutations. From the other three point mutations (M253I, D263E, and I264V) only the M253I shows a very minor positive influence on the binding affinity. For the further optimization of the Myc interference we predicted (based on rational design) and analyzed three further Mip mutants. Two of the three mutations (MipH260L and MipV264I) showed higher binding affinities calculated by MM-GBSA based on constraint MD simulations. These constraints were needed to confine the accessible conformational space. Secondary structure and thermal unfolding of the Mip mutants in complexes with Myc and as homodimers were measured by CD spectroscopy. The melting temperatures of the complex of Myc with MipV264I and MipH260L increased by 4 and 18 °C, respectively, compared to the complex of Myc with Mip, in excellent agreement with the predictions.

Especially MipH260L shows a very high potential for inactivation of Myc, and can therefore be used as starting point for further optimizations based on the computational as well as experimental protocols presented here.

Acknowledgements

The authors wish to thank Karin Schmidtkunz for help with experiments. This work was funded in the Emmy Noether program of the Deutsche Forschungsgemeinschaft (DFG Grant Ar 373/1-1, 1-2), and supported by the Excellence Initiative of the German Federal and State Governments (EXC 294).

References

1. Grandori C, Cowley SM, James LP, Eisenman RN. The Myc/Max/Mad network and the transcriptional control of cell behavior. *Annu. Rev. Cell Dev. Biol.* 2000; **16**: 653–699.
2. Nasi S, Ciarapica R, Jucker R, Rosati J, Soucek L. Making decisions through Myc. *FEBS Lett.* 2001; **490**: 153–162.
3. Nesbit CE, Tersak JM, Prochownik EV. MYC oncogenes and human neoplastic disease. *Oncogene* 1999; **18**: 3004–3016.
4. Felsher DW, Bishop JM. Transient excess of MYC activity can elicit genomic instability and tumorigenesis. *Proc. Natl. Acad. Sci. U.S.A.* 1999; **96**: 3940–3944.
5. Felsher DW, Bishop JM. Reversible tumorigenesis by MYC in hematopoietic lineages. *Mol. Cell* 1999; **4**: 199–207.
6. Jain M, Arvanitis C, Chu K, Dewey W, Leonhardt E, Trinh M, Sundberg CD, Bishop JM, Felsher DW. Sustained loss of a neoplastic phenotype by brief inactivation of MYC. *Science* 2002; **297**: 102–104.
7. Shachaf CM, Kopelman AM, Arvanitis C, Karlsson A, Beer S, Mandl S, Bachmann MH, Borowsky AD, Ruebner B, Cardiff RD, Yang Q, Bishop JM, Contag CH, Felsher DW. MYC inactivation uncovers pluripotent differentiation and tumour dormancy in hepatocellular cancer. *Nature* 2004; **431**: 1112–1117.
8. Amati B, Littlewood TD, Evan GI, Land H. The c-Myc protein induces cell cycle progression and apoptosis through dimerization with Max. *EMBO J.* 1993; **12**: 5083–5087.
9. Amati B, Brooks MW, Levy N, Littlewood TD, Evan GI, Land H. Oncogenic activity of the c-Myc protein requires dimerization with Max. *Cell* 1993; **72**: 233–245.
10. Amati B, Dalton S, Brooks MW, Littlewood TD, Evan GI, Land H. Transcriptional activation by the human c-Myc oncoprotein in yeast requires interaction with Max. *Nature* 1992; **359**: 423–426.
11. Ayer DE, Kretzner L, Eisenman RN. Mad: a heterodimeric partner for Max that antagonizes Myc transcriptional activity. *Cell* 1993; **72**: 211–222.
12. Ayer DE, Eisenman RN. A switch from Myc : Max to Mad : Max heterocomplexes accompanies monocyte/macrophage differentiation. *Genes Dev.* 1993; **7**: 2110–2119.
13. Blackwood EM, Eisenman RN. Max: a helix-loop-helix zipper protein that forms a sequence-specific DNA-binding complex with Myc. *Science* 1991; **251**: 1211–1217.
14. Dang CV, Resar LM, Emison E, Kim S, Li Q, Prescott JE, Wonsey D, Zeller K. Function of the c-Myc oncogenic transcription factor. *Exp. Cell Res.* 1999; **253**: 63–77.
15. Pelengaris S, Khan M. The many faces of c-MYC. *Arch. Biochem. Biophys.* 2003; **416**: 129–136.
16. Pelengaris S, Khan M, Evan G. c-MYC: more than just a matter of life and death. *Nat. Rev. Cancer* 2002; **2**: 764–776.
17. Wanzel M, Herold S, Eilers M. Transcriptional repression by Myc. *Trends Cell Biol.* 2003; **13**: 146–150.
18. Marchetti A, Abril-Marti M, Illi B, Cesareni G, Nasi S. Analysis of the Myc and Max interaction specificity with lambda repressor-HLH domain fusions. *J. Mol. Biol.* 1995; **248**: 541–550.
19. Ellenberger TE, Brandl CJ, Struhl K, Harrison SC. The GCN4 basic region leucine zipper binds DNA as a dimer of uninterrupted alpha helices: crystal structure of the protein-DNA complex. *Cell* 1992; **71**: 1223–1237.
20. O'Shea EK, Klemm JD, Kim PS, Alber T. X-ray structure of the GCN4 leucine zipper, a two-stranded, parallel coiled coil. *Science* 1991; **254**: 539–544.
21. Lupas AN, Gruber M. The structure of alpha-helical coiled coils. *Adv. Protein Chem.* 2005; **70**: 37–78.
22. Mason JM, Arndt KM. Coiled coil domains: stability, specificity, and biological implications. *ChemBioChem* 2004; **5**: 170–176.
23. Mason JM, Müller KM, Arndt KM. Considerations in the design and optimization of coiled coil structures. *Methods Mol. Biol.* 2007; **352**: 35–70.
24. Woolfson DN. The design of coiled-coil structures and assemblies. *Adv. Protein Chem.* 2005; **70**: 79–112.
25. Crick FHC. The packing of alpha-helices: simple coiled-coils. *Acta Crystallogr.* 1953; **6**: 689–697.
26. Wolf E, Kim PS, Berger B. MultiCoil: a program for predicting two- and three-stranded coiled coils. *Protein Sci.* 1997; **6**: 1179–1189.
27. Harbury PB, Zhang T, Kim PS, Alber T. A switch between two-, three-, and four-stranded coiled coils in GCN4 leucine zipper mutants. *Science* 1993; **262**: 1401–1407.
28. Harbury PB, Kim PS, Alber T. Crystal structure of an isoleucine-zipper trimer. *Nature* 1994; **371**: 80–83.
29. Woolfson DN, Alber T. Predicting oligomerization states of coiled coils. *Protein Sci.* 1995; **4**: 1596–1607.
30. Zhu BY, Zhou NE, Kay CM, Hodges RS. Packing and hydrophobicity effects on protein folding and stability: effects of beta-branched amino acids, valine and isoleucine, on the formation and stability of two-stranded alpha-helical coiled coils/leucine zippers. *Protein Sci.* 1993; **2**: 383–394.
31. Krylov D, Barchi J, Vinson C. Inter-helical interactions in the leucine zipper coiled coil dimer: pH and salt dependence of coupling energy between charged amino acids. *J. Mol. Biol.* 1998; **279**: 959–972.
32. Arndt KM, Pelletier JN, Müller KM, Plückthun A, Alber T. Comparison of in vivo selection and rational design of heterodimeric coiled coils. *Structure* 2002; **10**: 1235–1248.
33. O'Shea EK, Lumb KJ, Kim PS. Peptide 'Velcro': Design of a heterodimeric coiled coil. *Curr. Biol.* 1993; **3**: 658–667.
34. Marti DN, Jelesarov I, Bosshard HR. Interhelical ion pairing in coiled coils: solution structure of a heterodimeric leucine zipper and determination of pKa values of Glu side chains. *Biochemistry* 2000; **39**: 12804–12818.
35. Mason JM, Müller KM, Arndt KM. Positive aspects of negative design: simultaneous selection of specificity and interaction stability. *Biochemistry* 2007; **46**: 4804–4814.
36. Mason JM, Hagemann UB, Arndt KM. Improved stability of the Jun-Fos Activator Protein-1 coiled coil motif: A stopped-flow circular dichroism kinetic analysis. *J. Biol. Chem.* 2007; **282**: 23015–23024.
37. Mason JM, Schmitz MA, Müller KM, Arndt KM. Semirational design of Jun-Fos coiled coils with increased affinity: Universal implications for leucine zipper prediction and design. *Proc. Natl. Acad. Sci. U.S.A.* 2006; **103**: 8989–8994.
38. Arndt KM, Pelletier JN, Müller KM, Alber T, Michnick SW, Plückthun A. A heterodimeric coiled-coil peptide pair selected in vivo from a designed library-versus-library ensemble. *J. Mol. Biol.* 2000; **295**: 627–639.
39. Jouaux EM, Schmidtkunz K, Müller KM, Arndt KM. Targeting the c-Myc Coiled Coil with Interfering Peptides to Inhibit DNA Binding. *J. Pept. Sci.* 2008; **14**: 1022–1031.
40. Pelletier JN, Arndt KM, Plückthun A, Michnick SW. An in vivo library-versus-library selection of optimized protein-protein interactions. *Nat. Biotechnol.* 1999; **17**: 683–690.
41. Krylov D, Echlin DR, Taparowsky EJ, Vinson C. Design of dominant negatives to bHLHZip proteins that inhibit DNA binding. *Curr. Top. Microbiol. Immunol.* 1997; **224**: 169–177.
42. Krylov D, Kasai K, Echlin DR, Taparowsky EJ, Arnheiter H, Vinson C. A general method to design dominant negatives to B-HLHZip proteins that abolish DNA binding. *Proc. Natl. Acad. Sci. U.S.A.* 1997; **94**: 12274–12279.
43. Offer G, Sessions R. Computer modelling of the alpha-helical coiled coil: packing of side-chains in the inner core. *J. Mol. Biol.* 1995; **249**: 967–987.
44. Mohanty D, Kolinski A, Skolnick J. De Novo Simulations of the Folding Thermodynamics of the GCN4 Leucine Zipper. *Biophys. J.* 1999; **77**: 54–69.
45. Charest G, Lavigne P. Simple and versatile restraints for the accurate modeling of alpha-helical coiled-coil structures of multiple strandedness, orientation and composition. *Biopolymers* 2006; **81**: 202–214.

46. Pineiro A, Villa A, Vagt T, Koksch B, Mark AE. A molecular dynamics study of the formation, stability, and oligomerization state of two designed coiled coils: possibilities and limitations. *Biophys. J.* 2005; **89**: 3701–3713.
47. Lee H, Larson RG. Prediction of the stability of coiled coils using molecular dynamics simulations. *Mol. Simul.* 2007; **33**: 463–473.
48. Danciulescu C, Nick B, Wortmann F-J. Structural stability of wild type and mutated α-keratin fragments: Molecular dynamics and free energy calculations. *Biomacromolecules* 2004; **5**: 2165–2175.
49. Missimer JH, Seinmetz MO, Baron R, Winkler FK, Kammerer RA, Daura X, van Gunsteren WF. Configurational entropy elucidates the role of salt-bridge networks in protein thermostability. *Protein Sci.* 2007; **16**: 1349–1359.
50. Laughton CA, Luisi BF, Pratap JV, Calladine CR. A Potential Molecular Switch in an α-Helical Coiled Coil. *Proteins: Struct., Funct., Bioinf.* 2008; **70**: 25–30.
51. Gohlke H, Kiel Ch, Case DA. Insights into protein-protein binding by binding free energy calculation and free energy decomposition for the Ras-Raf and Ras-RalGDS complexes. *J. Mol. Biol.* 2003; **330**: 891–913.
52. Gohlke H, Case DA. Converging free energy estimates: MM-PB(GB)SA studies on the protein-protein complex Ras-Raf. *J. Comput. Chem.* 2004; **25**: 238–250.
53. Gohlke H, Kuhn LA, Case DA. Change in protein flexibility upon complex formation: Analysis of Ras-Raf using molecular dynamics and a molecular framework approach. *Proteins: Struct., Funct., Bioinf.* 2004; **56**: 322–337.
54. Kollman PA, Massova I, Reyes C, Kuhn B, Huo S, Chong L. Calculation structures and free energies of complex molecules: combining molecular mechanics and continuum models. *Acc. Chem. Res.* 2000; **33**: 889–897.
55. Srinivasan J, Cheatham TEI, Cieplak P, Kollman PA, Case DA. Continuum solvent studies of the stability of DNA, RNA, and phosphoramidate-DNA helices. *J. Am. Chem. Soc.* 1998; **120**: 9401–9409.
56. Cornell WD, Cieplak CI, Bayly IR, Gould IR, Merz KM, Ferguson DM, Spellmeyer DC, Fox T, Caldwell JW, Kollman PA. A second generation force field for the simulation of proteins, nucleic acids, and organic molecules. *J. Am. Chem. Soc.* 1995; **117**: 5179–5197.
57. Jayaram B, Sprouse D, Beveridge DL. Solvation free energy of biomolecules: parameters for a modified generalized born model consistent with the AMBER force field. *J. Phys. Chem. B* 1998; **102**: 9571–9576.
58. Weiser J, Shenkin PS, Still WC. Approximate atomic surfaces from linear combinations of pair-wise overlaps. *J. Comput. Chem.* 1999; **20**: 217–230.
59. Case DA, Darden TA, Cheatham TEI, Simmerling CL, Wang J, Duke R, Luo KM, Merz KM, Wang B, Pearlman DA, Crowley M, Brozell S, Tsui V, Gohlke H, Morgan J, Hornak V, Cui G, Beroza P, Schafmeister C, Caldwell JW, Ross WS, Kollman PA. AMBER8, University of California, San Francisco, 2004.
60. Berman HM, Westbrook J, Feng Z, Filliland G, Bhat TN, Weissig H, Shindyalov IN, Bourne PE. The protein data bank. *Nucleic Acids Res.* 2000; **28**: 235–242.
61. Jorgensen WL, Chandrasekhar J, Madura J, Klein ML. Comparison of simple potential functions for simulating liquid water. *J. Chem. Phys.* 1983; **79**: 926–935.
62. Darden T, York D, Pedersen L. Particle mesh ewald – A Nlog(N) method for ewald sums in large systems. *J. Chem. Phys.* 1993; **98**: 10089–10092.
63. Ryckaert JP, Ciccotti G, Berendsen HJC. Numerical integration of cartesian equations of motion of a system with constraints – molecular dynamics of n-alkanes. *J. Comput. Phys.* 1977; **23**: 327–341.
64. Becktel WJ, Schellman JA. Protein stability curves. *Biopolymers* 1987; **26**: 1859–1877.
65. Arndt KM, Pelletier JN, Müller KM, Plückthun A, Alber T. Comparison of in vivo selection and rational design of heterodimeric coiled coils. *Structure (Camb)* 2002; **10**: 1235–1248.
66. O'Shea EK, Rutkowski R, Kim PS. Mechanism of specificity in the Fos-Jun oncoprotein heterodimer. *Cell* 1992; **68**: 699–708.
67. Krylov D, Mikhailenko I, Vinson C. A thermodynamic scale for leucine zipper stability and dimerization specificity: e and g interhelical interactions. *EMBO J.* 1994; **13**: 2849–2861.
68. Monera OD, Zhou NE, Kay CM, Hodges RS. Comparison of antiparallel and parallel two-stranded alpha-helical coiled-coils. Design, synthesis, and characterization. *J. Biol. Chem.* 1993; **268**: 19218–19227.
69. Lavigne P, Kondejewski LH, Houston ME Jr, Sönnichsen FD, Lix B, Sykes BD, Hodges RS, Kay CM. Preferential heterodimeric parallel coiled-coil formation by synthetic Max and c-Myc leucine zippers: a description of putative electrostatic interactions responsible for the specificity of heterodimerization. *J. Mol. Biol.* 1995; **254**: 505–520.
70. Lavigne P, Crump MP, Gagne SM, Hodges RS, Kay CM, Sykes BD. Insights into the mechanism of heterodimerization from the ^{1}H-NMR solution structure of the c-Myc-Max heterodimeric leucine zipper. *J. Mol. Biol.* 1998; **281**: 165–181.
71. Nair SK, Burley SK. X-ray structure of Myc-Max and Myd-Max recognizing DNA. Molecular bases of regulation by proto-oncogenic transcription factors. *Cell* 2003; **112**: 193–205.
72. Montagne M, Naud J-F, McDuff F-O, Lavigne P. Toward the elucidation of the structural determinants responsible for the molecular recognition between Mad1 and Max. *Biochemistry* 2005; **44**: 12860–12869.
73. Montagne M, Naud J-F, Lavigne P. Elucidation of the structural determinants responsible for the specific formation of heterdimeric Mxd1/Max b-HLH-LZ and its binding to E-box sequences. *J. Mol. Biol.* 2008; **376**: 141–152.

